Technische Universität München

Physik-Department

Bachelor Thesis in Physics

Tracking studies with silicon detectors for the HADES Pion Tracker

Tobias Schmitt

Supervisors: Prof. Dr. Laura Fabbietti, Rafał Lalik

Contents

1 Introduction

HADES Spectrometer

The **H**igh **A**cceptance **D**i-**E**lectron **S**pectrometer (HADES) is a fixed target experiment located at the SIS18, in GSI[1] Darmstadt, Germany. It was built to study e^+e^--pairs (di-electrons) and charged hadrons produced in proton, pion and heavy ion collisions at beam energies up to 3.5 GeV. The main experimental goal is to study the production of scalar and vector mesons with strangeness.

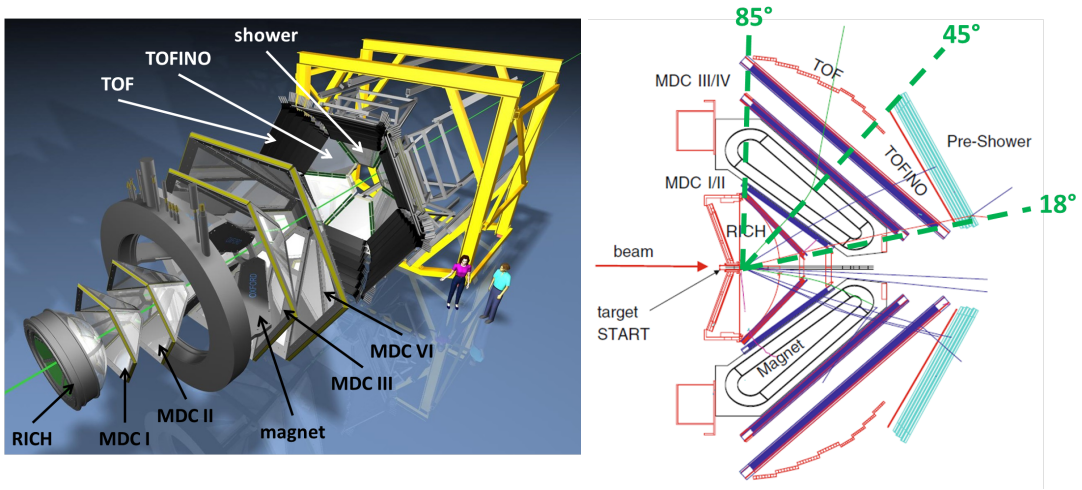

Figure 1.1: The HADES spectrometer setup with all detectors. Left an schematic overview, except TOFINO/RPC. TOFINO/RPC is in front of the shower detector between 18° and 45° in forward direction. Right a cross section of the detector [1].

The spectrometer consists of several sub detectors, covering an angle between 18° and 85° in the forwards direction and the full azimuthal range [1] (fig. 1.1).
The beam first hits the START detector, to get a start signal for each incoming particle, and then the target. After that there is the RICH[2] detector for electron-hadron separation. Then come four multi-wire drift-chambers (MDC) with a magnet after the first two, to reconstruct the tracks and the momentum. To complete the particle identification there is a time of flight (TOF) measurement in HADES. This is achieved by the TOF/TOFINO wall together with the start signal from the START detector. The TOFINO detector had been replaced in an upgrade by the high-granularity timing Resistive Plate Chamber (RPC) to get a better time resolution. At the end is a shower detector.

[1] Schwerionensynchrotron18; GSI Helmholtzzentrum für Schwerionenforschung
[2] **R**ing-**I**maging-**CH**erenkov-Detektor

Physics Motivation for Pion Experiments

A special interest is dedicated to the production on strange baryonic (Λ, Σ, ...) and mesonic (K^0, ϕ, ...) matter, which can be created in pion induced reactions. Together with nuclear matter they can strike up a bound state, which betrays something about the predominant processes in nuclear matter. One of these effects is, for example, a shift of the effective mass of the strange particle in the vicinity of other nucleons. Up to now strangeness in nuclear matter had been studied at HADES in proton-proton, proton-nucleon and nucleon-nucleon collisions. To get more precise information and easier manageable results, π-p and π-nucleon collisions are planned. The pions will collide with a liquid hydrogen (LH_2) target and three solid targets. For those, one with a light (carbon), one with a medium (copper) and one with a heavy (tungsten) nucleus will be used.
The results are applicable in the description of neutron stars. Due to their extreme high density in the inner of the star it is energetically possible to produce strangeness, since the Fermi pressure is relieved. There, again, the effects of strange matter in nuclear matter would play an important role. The mass shift would have a decreasing effect on the maximum mass of such a star [2].

Pion Beam

To get a pion beam, the pions have to be produced in a primary reaction. For this, particles will be shot onto a production target, where they will be created. Since the pions are a secondary beam, momentum and angle will have a big spread. Via beam optics, a certain range of them will be selected and reaches the HADES target. The momentum for each particle is different and lies within $\pm 8\%$ of the central momentum p_0. Hence the momentum has to be measured with at least 0.5% precision. This will be done with the CERBEROS[3] detector. It has to handle rates of up to $2 \cdot 10^8$ particles per second (10^6 of them are pions, the rest is background).
This system consists of two silicon detectors located at two different positions (figs. 1.2 and 1.3), measuring the x- and y-coordinate of the particle hit. Using beam optics and a transport approach, one can calculate with these four coordinates the momentum of each pion [3].

The silicon detectors are going to be located in a $32 \times 32 \times 12$ cm^3 vacuum chamber out of aluminium (fig. 1.4). Tests[4] showed that pressures down to 10^{-8} mbar can be achieved. This is sufficient for the two operational areas, NE5 and the HADES cave[5]. Heating has a negative influence on the signal to noise ratio and the radiation hardness, thus the silicon is going to be cooled [4] [5].
In fig. 1.4 a CAD model of the vacuum chamber with detector, cooling and front end boards can be seen. The hole on the bottom will be connected to the beam line.

[3] **CE**nt**R**al **BE**am t**R**acker for pi**O**n**S**
[4] Carried out by author in lab in Munich and by Technology Lab at GSI.
[5] NE5 area is directly after the pion production target and the HADES are the last few meters before the target.

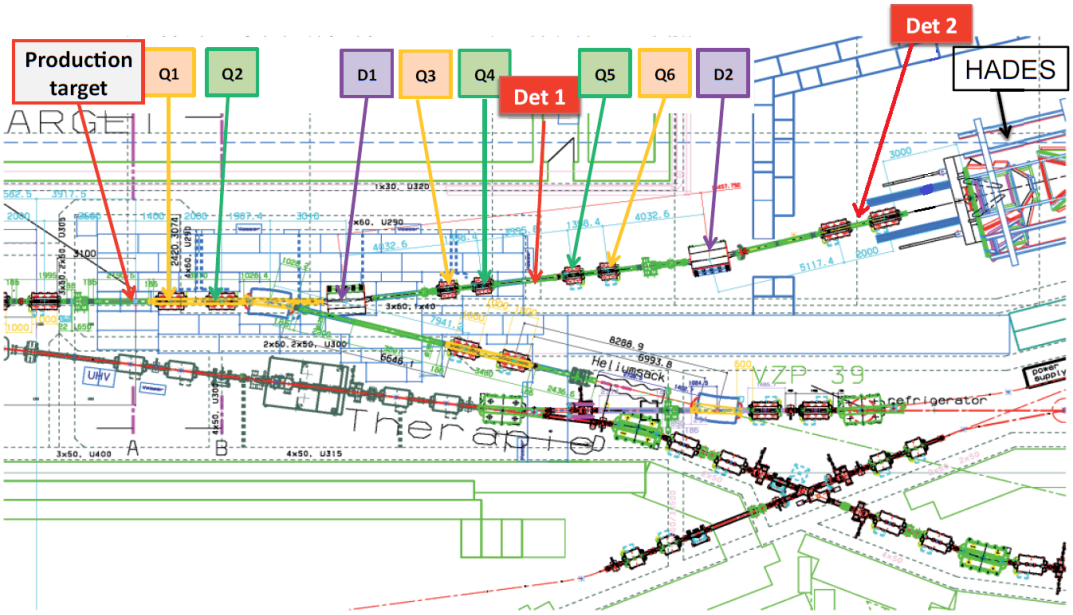

Figure 1.2: Technical drawing of the HADES part of the beam line. Pions come from the production target and go to the HADES spectrometer. The first detector will be located in the NE5 area around 17 m and the second one is in the HADES cave around 5 m in front of the target. The NE5 area is between the production target and dipole D2. Everything behind corresponds to the HADES cave. Some changes in the quadrupole positions have been made but are not relevant here. Picture made by Thierry Hennino [3].

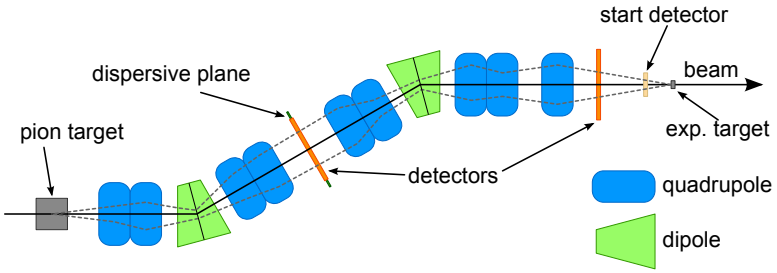

Figure 1.3: Sketch of the HADES beam line. The beam comes from the left and hits the pion production target. The created pions travel along the beam line to the HADES spectrometer. The dashed lines illustrate the widening and focusing of the beam by the quadrupoles (blue) and dipoles (green). The small orange lines are the the Pion Trackers. They provide a spatial measurement of the particle position. With that one can deduce the particle's momentum.

A prototype of this system was tested at GSI in November 2012. During these tests, the silicon detectors were neither in a vacuum, nor were they cooled. These measurements were meant to test the DAQ[6] and the MIP[7] triggering capability of the system. For this thesis the angular distributions of incident particles and their energy deposit in the

[6] **D**ata **AQ**uisition
[7] **M**inimal **I**onizing **P**article

detector were also important. Calculations[8] showed that the pions will traverse the detector between an angle of 0° and 1.2°, so nearly perpendicular. This is shown on fig. 6.1 and fig. 6.2 in the appendix. Despite of the small angle, there is a non vanishing probability for particles to deposit their energy in two neighbouring strips (fig. 1.5). Thus the signal is split up into two parts. This could lead to signals below the threshold and the hit information would be lost.

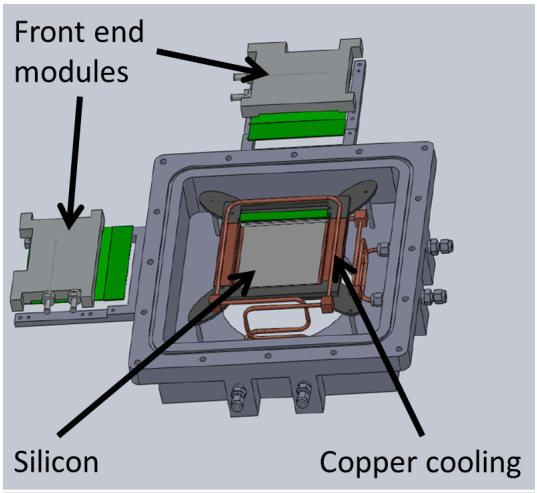

Figure 1.4: CAD picture of one half of the vacuum chamber with the detector in the middle. The cooling is mounted on the detector and the front end modules are located on two sides of the chamber [3].

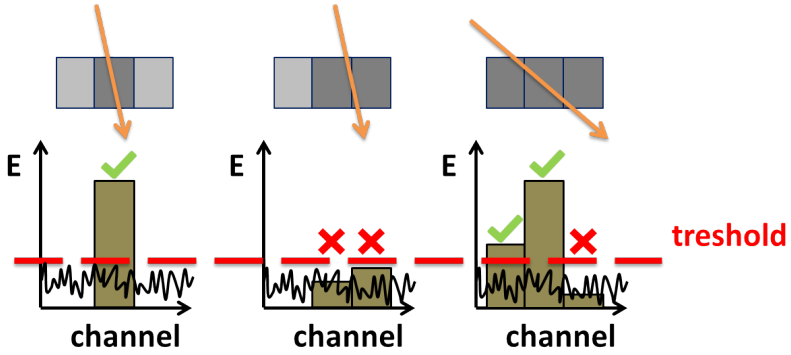

Figure 1.5: Particles going through strips are depositing energy there. If the energy deposit is above a threshold, a hit will be detected, otherwise the hit information gets lost.

This is especially relevant for the CERBEROS detector because the readout is internally triggered on the signal amplitude of each strip. The data is then sent to the HADES DAQ, where only relevant events, in coincidence to events in HADES, are stored to disk.
Furthermore a deeper analysis of the angle dependency is useful for potential later applications of silicon strip detectors in particle tracking.

[8] Made by Thierry Hennino; Institut de Physique Nucléaire, Université Paris Sud, F-91406 Orsay Cedex, France.

2 The Test Setup

During the tests at GSI, data with $8.6 \cdot 10^5$ events had been recorded. They correspond to several runs, between which small changes in the setup were made. Only two of them were analysed, from here on denoted as run D and run K.
In table 2.1 the most important properties of the two relevant runs are summarized. The efficiency seems to be lower than expected. This will be discussed in section 4.3.

	run D	run K
# trigger events	234399	506893
# reconstructed tracks	153488	291401
track efficiency	86.4%	71.4%
orientation of scintillator	horizontal	vertical
beam particle	^{2}H	^{2}H
beam energy	1.9 GeV	1.9 GeV
target	1 mm aluminium	1 mm aluminium
beam intensity	377 kHz	2.29 - 9.56 MHz
average trigger intensity	170 Hz	48 - 600 Hz
maximal trigger intensity	410 Hz	600 Hz

Table 2.1: All relevant properties of the two runs. Run K has roughly twice the data of run D. The track efficiency is the number of reconstructed tracks divided by the number of events in coincidence on all four n-XYTER.

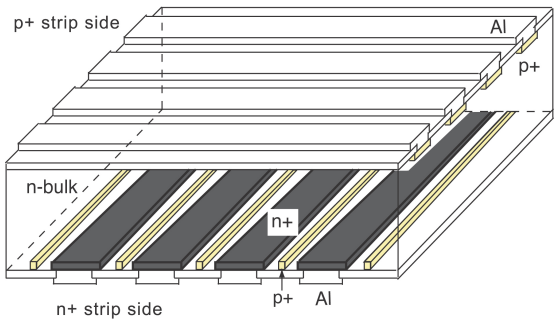

Figure 2.1: Schematic drawing of a double sided silicon detector [6]. P-side is on the top and n-side is on the bottom, in between is silicon. The strips are the doped regions on the p- and n-side.

The test setup consisted of two Micron Semiconductors TTT3 silicon sensors [7], called Det1 and Det2. Each of them is a 100.42×100.42 mm^2 double sided silicon detector with 128 strips on each side and 300 μm thickness (fig. 2.1), located in a light tight box of aluminium. In these tests the detectors were not cooled.
The detectors were read out by front end boards (FEB) based on the n-XYTER[9] ASIC[10]. N-XYTER 2 (Nx2) and n-XYTER 3 (Nx3) were n- and p-side of the first detector and n-XYTER 0 (Nx0) and n-XYTER 1 (Nx1) were n- and p-side of the second detector (fig. 2.2).

[9] **n**eutron-**X**,**Y**, **T**ime and **E**nergy **R**eadout
[10] **A**pplication-**S**pecified **I**ntegrated **C**ircuit

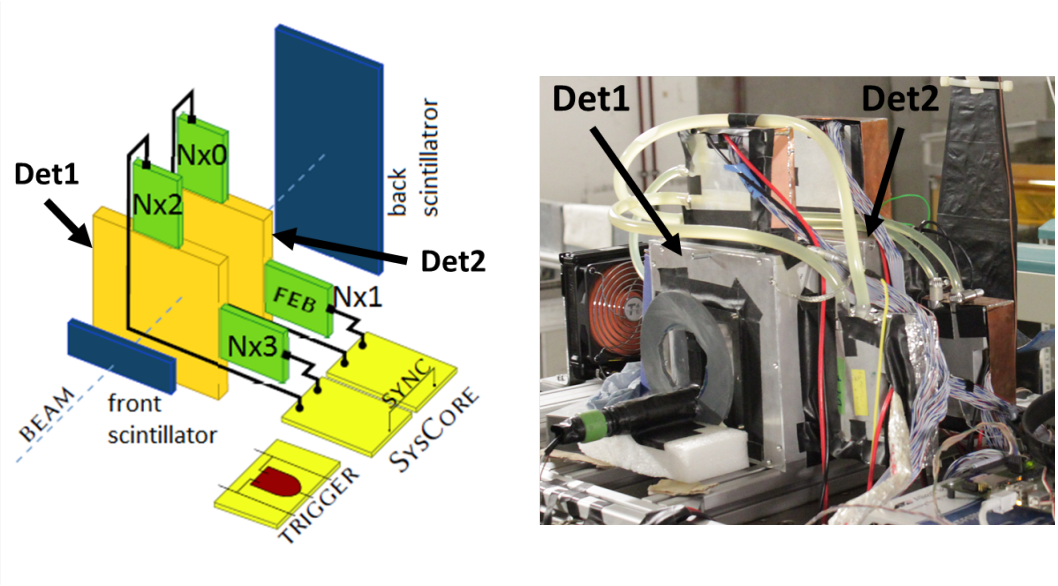

Figure 2.2: Configuration of the test setup. Left: The two detectors Det1 and Det2. The n-XYTER 0 and 2 are the readout for the x-coordinate and n-XYTER 1 and 3 the readout for the y-coordinate. The collected data goes to the SysCore board, which handles it together with up to 4 different trigger modes and saves it to a hard drive. The trigger signal comes from the two scintillators [3]. Right: Picture of the test setup. Detector 1 and 2 were in aluminium boxes. The scintillators are on the front and back side of the detectors, wrapped in black tape.

For the test, the internal threshold of the n-XYTER readout was set straight above the noise. A trigger was produced by the back and front scintillator, to ensure a particle passed the two detectors. There had been three different possibilities to trigger a signal: only the front, or the back scintillator, or the coincidence of both. In this thesis only the last trigger configuration is analysed, so it can be guaranteed that the tracks of the particles really went through the detector system and were not scattered away. Also, the inclination angle of the particles can be determined.

The front scintillator had a size of 20×60 mm^2 and the back scintillator 115×250 mm^2. So the front scintillator was significantly smaller than the detector area, whereas the back scintillator was big enough to cover the whole detector area. Both were plastic scintillators on the base of ployvinyltoluene (BC-408) with a refraction index of 1.58 and an absorption length of 210 cm [8].

The system was located in the FOPI[11] cave at GSI in Darmstadt. It was a fixed target experiment with 1.9 GeV deuteron beam impinging on different targets. The detector setup was around 10 m behind the target and shifted from the beam axis by around 50 cm to avoid heavy fragment hits. Thus mostly secondary protons and pions have been measured. The detector planes were not perpendicular to the beam axis, but aligned to the target with a small inclination angle to the beam axis. There were also some other experiments, which were directly in the beam line (fig. 2.3), which turned out to be additional sources of particles as it will be shown in section 4.1.

[11] FOPI stands for 4π and is a detector for heavy ion collisions at GSI

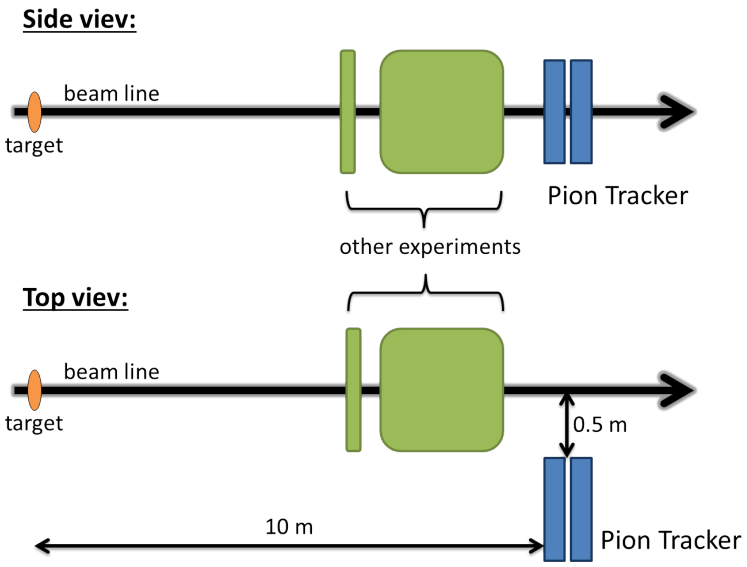

Figure 2.3: The whole test setup in the FOPI cave. The beam comes from the left and hits the target in FOPI. The two blue boxes are the Pion Tracker, which is shifted around 50 cm from the beam axis. The green boxes are other experiments, which were directly in the beam line.

3 Raw Data Analysis

3.1 Cluster Reconstruction

Definitions

First a few terms have to be defined. The cluster size (CS) is the distance between the two outermost fired strips. The number of fired strips in an event is the strip multiplicity (SM). One can deduce from those two to the hit multiplicity (HM). If the cluster size is equal to the strip multiplicity, then the hit multiplicity is 1 (fig. 3.1 a) and b)). If it is bigger than the strip multiplicity, then the event can be split up in several sub clusters, which leads to a higher hit multiplicity (fig. 3.1 c)).

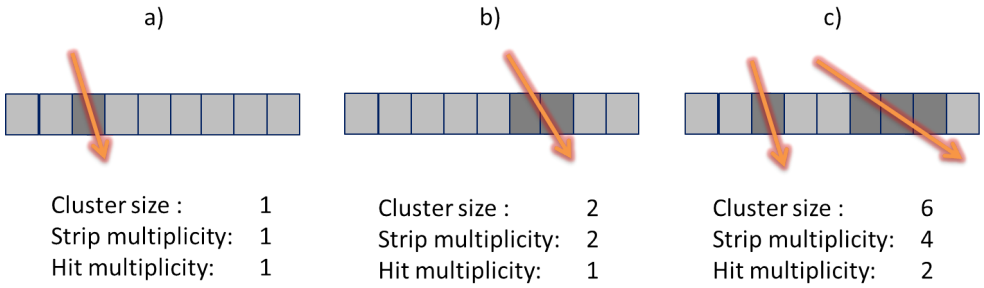

Figure 3.1: Explanation of strip multiplicity, hit multiplicity and cluster size.

It has to be considered that the hit multiplicity is not always the correct number of hits. There are several error sources like noise above the threshold and particles crossing the detector nearby. In the first case a fake hit is created, and in the second case two particle hits are registered as one. To get rid of most of these errors, only events with hit multiplicity 1 are kept for the following analysis.

Analysis

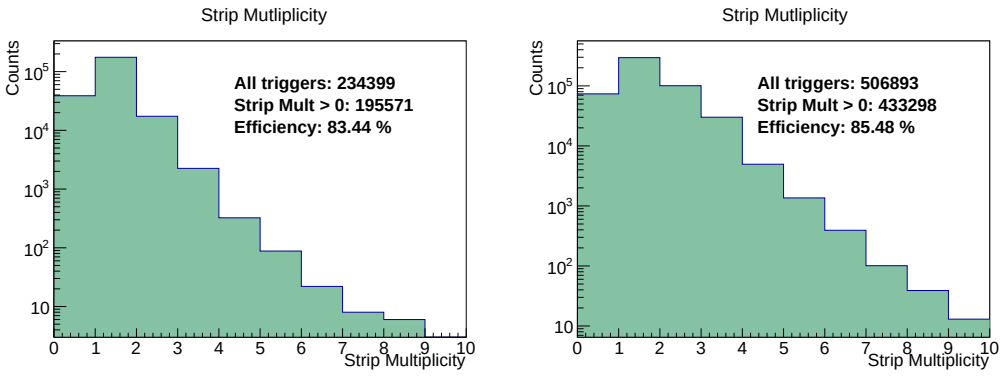

Figure 3.2: Strip multiplicity for Nx0 in run D (left) and run K (right). Efficiency is calculated by dividing the number of events with at least 1 fired strip by the total number of events.

The strip multiplicity plot (fig. 3.2) provides information about the number of fired strips per event. All hit multiplicities were taken into account for this. The fraction of events with 0 strip multiplicity gives a first measurement of the efficiency of each n-XYTER. The extracted values are listed in table 3.1. The real efficiency of the detector will be calculated in section 4.3.

	run D	run K
Nx0	83.44%	85.48%
Nx1	85.09%	84.89%
Nx2	93.45%	92.74%
Nx3	94.44%	94.39%

Table 3.1: Efficiency of each n-XYTER. The values are so low, because not all triggered particles went through the detectors and both detectors had broken strips.

Figure 3.3 shows the histograms with the cluster sizes in events with different strip multiplicity for run D.

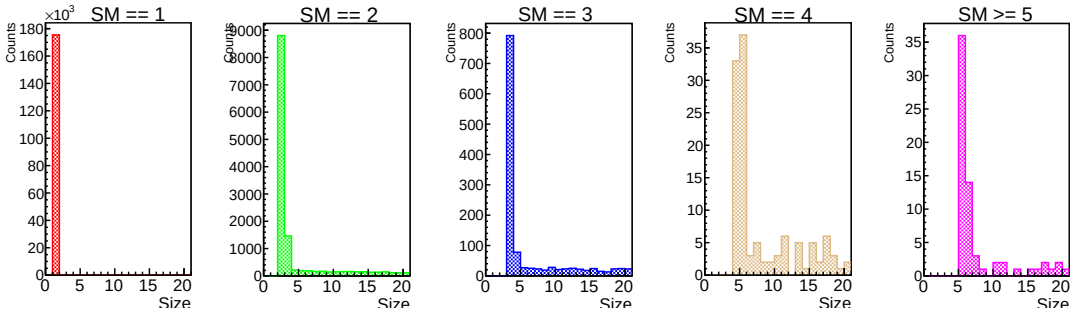

Figure 3.3: The histograms show the number of events with a certain cluster size for the different strip multiplicity. The histograms are ordered from the left to the right for increasing strip multiplicity. The picture shows run D. Run K looks similar.

From figs. 3.2 and 3.3 one can imply that most of the events have clusters with size 1 or 2 in run D and clusters with size 1, 2 or 3 for run K. So the whole analysis will focus on the cluster sizes 1, 2 and 3.

3.2 Particle Energy Loss

The standard Bethe-Bloch curve, given by:

$$\frac{\mathrm{d}E}{\mathrm{d}x} \propto \frac{z^2}{\beta^2} \cdot \left[\ln\left(\frac{2\mathrm{m_e}c^2\beta^2}{\mathrm{I}\cdot(1-\beta^2)} \right) - \beta^2 \right] \tag{3.1}$$

$\beta = v/c$
z = charge of the particle
I = mean excitation potential of the material

describes the energy loss of a charged particle in matter. With higher energy the probability to knock out electrons from the material increases. Those electrons are called

delta electrons. The energy they carry away can not be detected. This leads to the restricted curve, which describes the measurable energy loss.

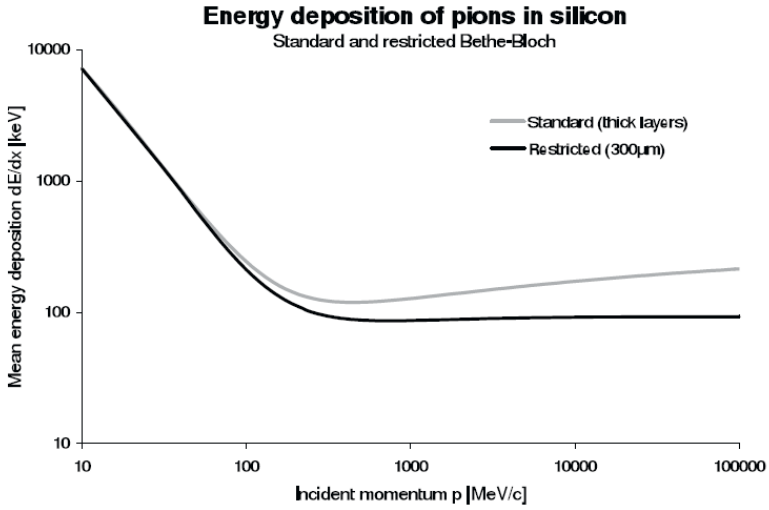

Figure 3.4: Bethe-Bloch formula for pions. The restricted curve counts for a thin layer of silicon. This curve has a shifted minimum and a quite flatter rise at relativistic energies, because of delta electrons [9].

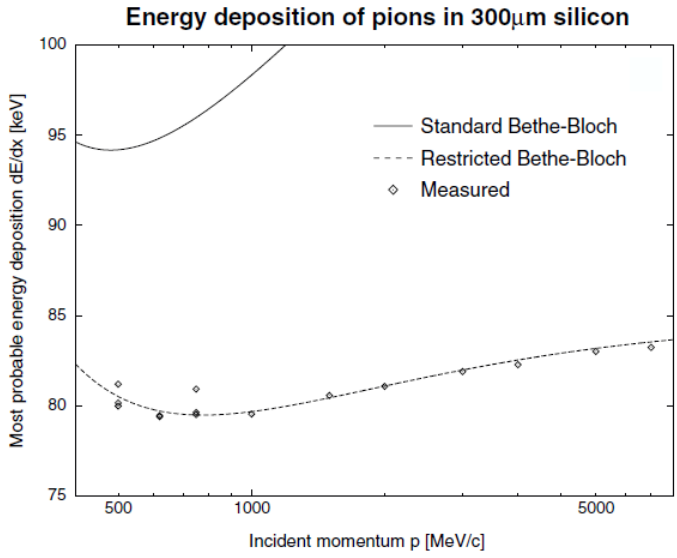

Figure 3.5: Bethe-Bloch formula for pions with a zoom in the MIP region. The picture shows a measurement for the restricted curve, done by the CMS collaboration [9].

Since the particles of interest are pions in the pion beam experiment, we deal with MIPs. Such MIPs have also been measured mainly in the experiment at GSI in November. Pions have a mass of 139,57 MeV/c^2, this means that they need at least around 330 MeV kinetic energy (Gamma factor $\gamma \approx 3.37, \beta \approx 0.95$) to be a MIP. For a thin layer, where delta electron effects occur (compare fig. 3.4) the minimal ionizing region is at

approximately 623 MeV kinetic energy (Gamma factor $\gamma \approx 5.46, \beta \approx 0.98$). For minimal ionizing protons with the same β, the kinetic energy would be around 2.37 GeV for normal energy loss and 4.46 GeV for thin layers. As a consequence for this experiment, pions were in the MIP region and protons were in a region, where they deposited more energy. The protons were more ionizing, because the beam energy was only 1.9 GeV, and so the kinetic energy of them had to be lower than 4.46 GeV.
Figures 3.4 and 3.5 show the real and measurable energy loss of pions. Here the mean energy deposited in 300 μm silicon is shown as a function of the particle momentum. One can see that the measurable energy loss of minimal ionizing pions in 300 μm silicon is around 80 keV.

3.3 Baseline Correction

The pedestals were taken with a pulser of 1 kHz. In the test trigger mode the discriminator was forced to take data without the threshold selections. This provides the possibility to measure the noise. On the left side of fig. 3.6 a typical pedestal spectrum is shown. The ADC value is plotted against the channel number. The channel number is a readout channel of the n-XYTER, which corresponds to a strip. The curved structure comes from the internal structure of the n-XYTER and the geometry of the connection between detector and ASIC. To calibrate the detector readout, the mean of the ADC value for each channel was extracted and shifted to zero.

The noise is calculated via the sigma of the pedestal distribution. The mean of the noise is at around 11 ADC units, which corresponds to approximately 2000 electrons (fig. 3.6 right).

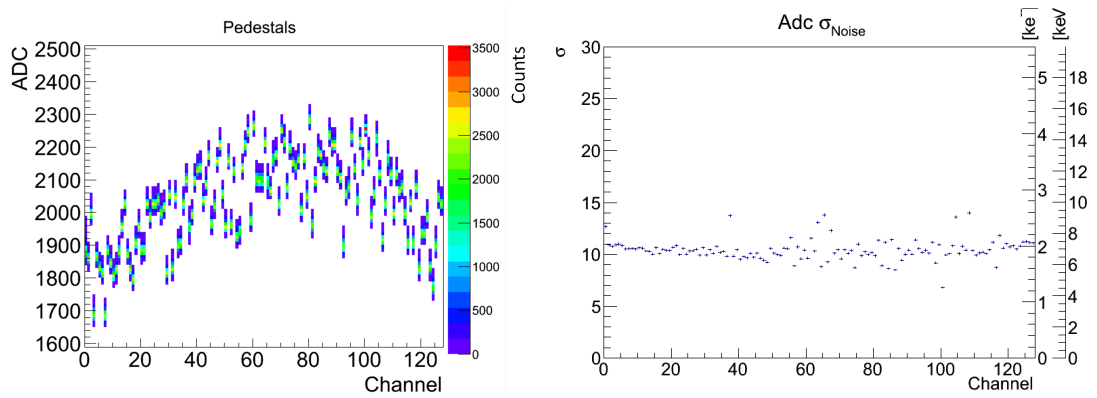

Figure 3.6: Left: Typical pedestal pattern for the detector. Here the pedestals for run D second detector x-direction (Nx0) are shown. All the others look similar. Right: Typical noise spectrum for the detector. The noise is plotted against the channel number (strips). Here it is shown for run D second detector x-direction (Nx0). All the others look similar.

3.4 Energy Spectrum for MIPs

Figure 3.7 shows an energy spectrum recorded during the experimental campaign at GSI. The peak, showed here for cluster sizes 1 and 2, is associated with an 80 keV MIP signal. The signal corresponding to "size 1" clusters was fitted with a Langau function (Landau convoluted with a Gaussian), thus the peak value is slightly shifted to higher values than the most probable value of the Landau distribution. The FWHM[12] is 114.0 ADC units. This leads to an energy resolution of FWHM/E $\approx$ 85%, that is rather large in comparison to the resolution of 50%, achieved by the CMS[13] experiment [3]. This value might be improved by better treatment of baseline corrections.
The noise peak is not seen here, because of the internal threshold of the n-XYTER. This shows also that the MIP signal can be separated from the noise.

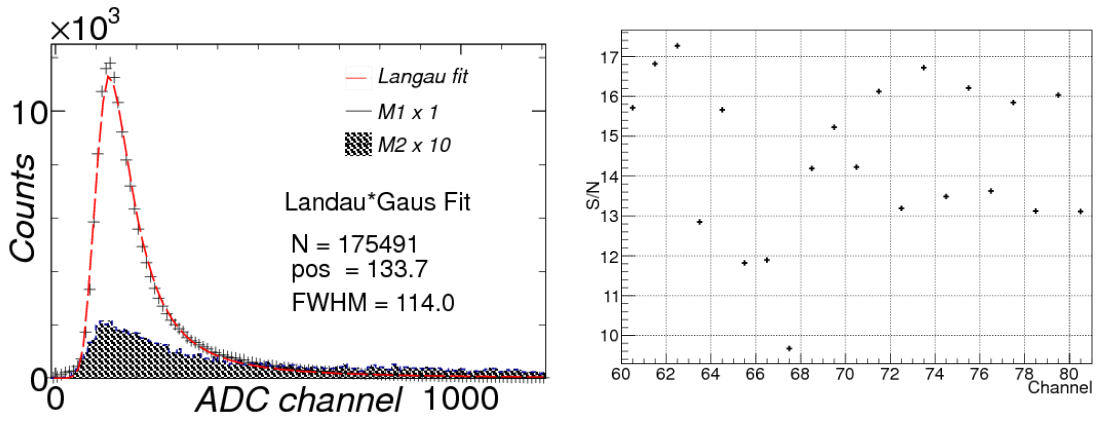

Figure 3.7: Left: Typical MIP signal for a single strip. cluster size 1 and 2 are shown together with a Langau fit (red) of cluster size 1 [10]. Right: Signal to noise ratio for some channels of a n-XYTER.

The signal to noise ratio (fig. 3.7 right) is calculated by dividing the mean value of a MIP signal by the sigma of the noise. The mean of all channels lies at around 14.

In the hit correlation plot (figs. 3.8 and 3.9) the x- and y-coordinate of each hit is extracted and filled into a two dimensional histogram. The white lines in the plots are caused by broken strips. The edges of the scintillator shape on Det1 look quite sharp, whereas on Det2 they look blurry. This is caused by the fact that there was more than only one target in the beam line. This is also the reason for the shift of the shadow in these plots. More precise analysis of this follows in section 4.1.

[12] **F**ull **W**idth at **H**alf **M**aximum
[13] **C**ompact **M**uon **S**olenoid

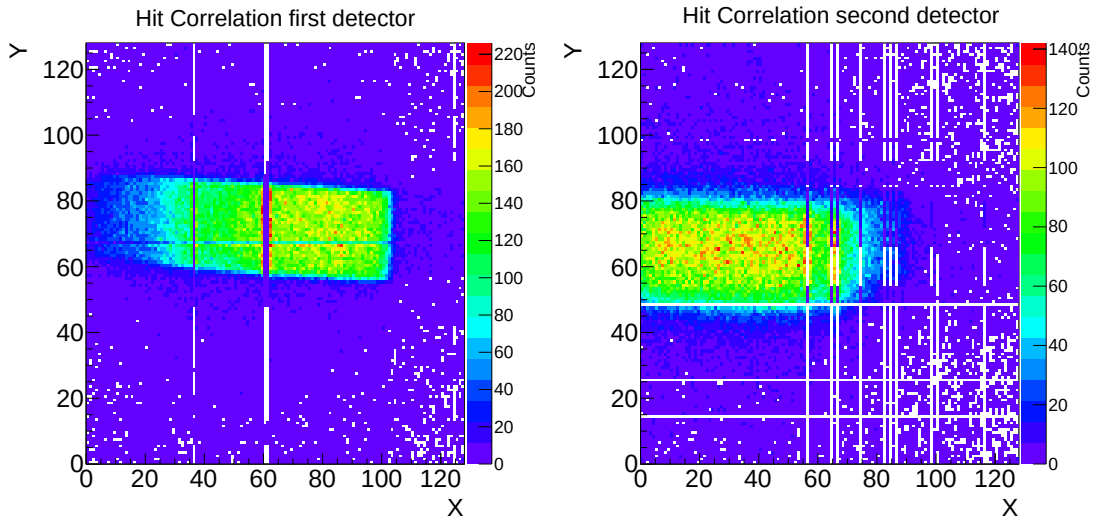

Figure 3.8: Hit correlation for the first detector (left) and the second detector (right) in run D. One can see the shape of the front scintillator and a shift in mainly the x-direction. The lines with zero (white) or a few (purple) events are broken strips.

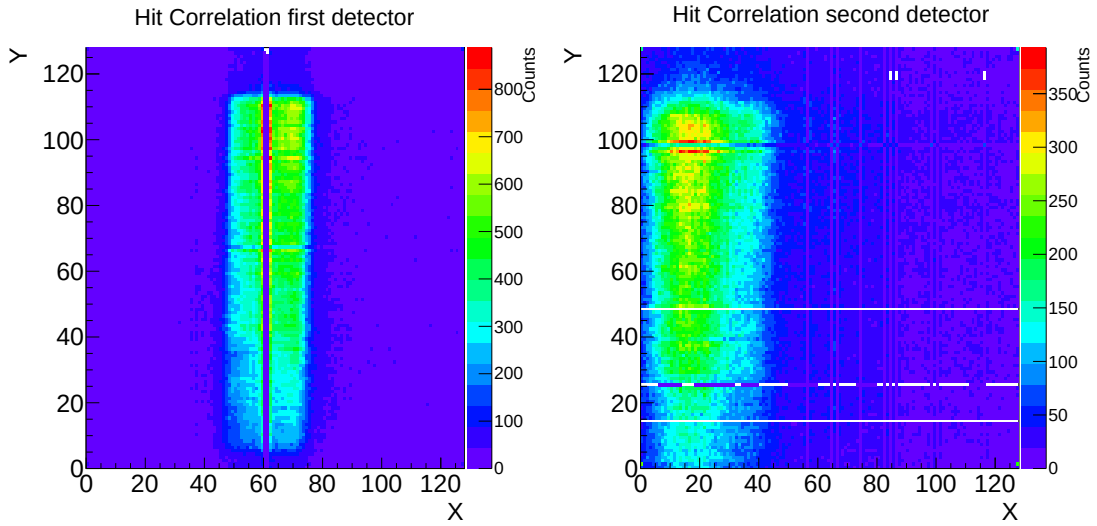

Figure 3.9: Hit correlation for the first detector (left) and the second detector (right) in run K. One can see the shape of the front scintillator and a shift in mainly the x-direction. The lines with zero (white) or a few (purple) events are broken strips.

4 Tracking

4.1 Track Reconstruction Analysis

The first step of the analysis consists of determining the incident angle of the incoming particle. To extract this information, the x and y positions for the particle hit on both detectors are compared (fig. 4.1 and eq. (4.1)). The Δx and Δy are plotted against each other. A peak is expected in correspondence of particles which are coming from the FOPI target at around (0,0). Small deviations in the alignment would cause a small shift from (0,0).

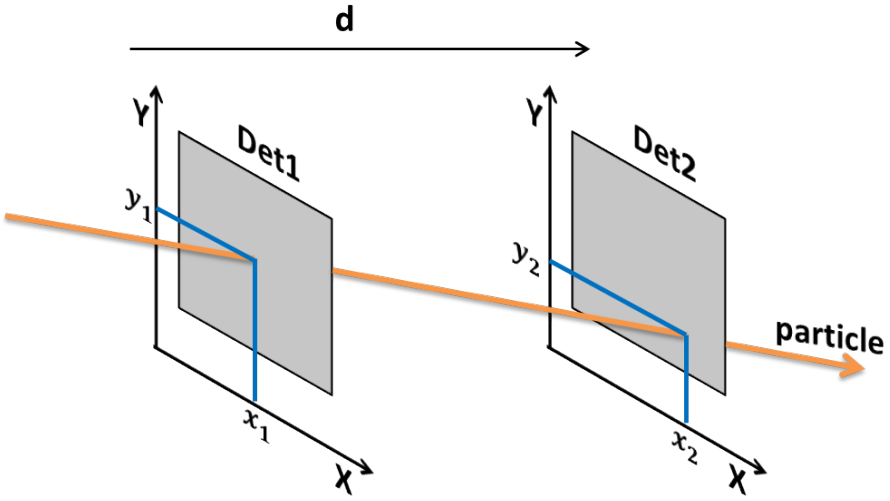

Figure 4.1: Scheme of track reconstruction procedure. The x and y position of the hit on each silicon detector are taken to calculate the track vector of each particle. This can be done with the distance d of the two detectors and the difference of the hit positions via eqs. (4.1) and (4.2).

$$\begin{aligned} \Delta x &= x_2 - x_1 \\ \Delta y &= y_2 - y_1 \end{aligned} \tag{4.1}$$

The position correlation of the hits on the first and the second detector, for beams D and K are shown on the left and right side of fig. 4.2. Because the detector was aligned to the FOPI target the main correlation peak (coming from this target) should be at position (0,0) – denoted as $T_0^{D,K}$ [14]. The presence of other peaks is a clear evidence for other particle sources at certain angles. They are marked as $T_{1...3}^{D,K}$. They were identified as particles coming from a secondary production or beam scattering on the other detectors located in the beam line in the experimental cave (figs. 2.3 and 4.3). In the later analysis the impact angle for these sources is measured. This information is important for the further analysis of the detected particles.

[14] Upper index refer to the run name.

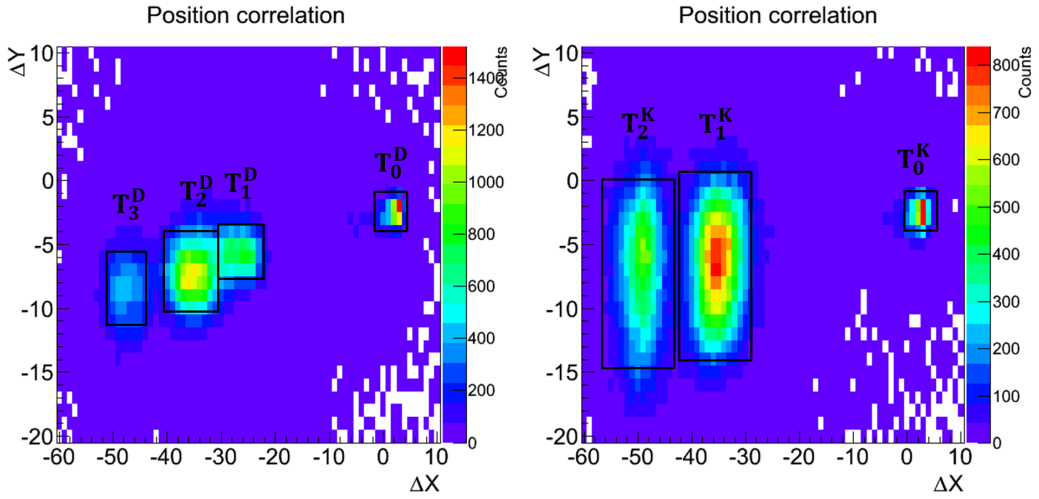

Figure 4.2: Position correlation for run D (left) and run K (right). Only events with CS1 are plotted. The different peaks correspond to different targets in the beam line. The black boxes illustrate the cuts around the peaks, which will be used in the later analysis.

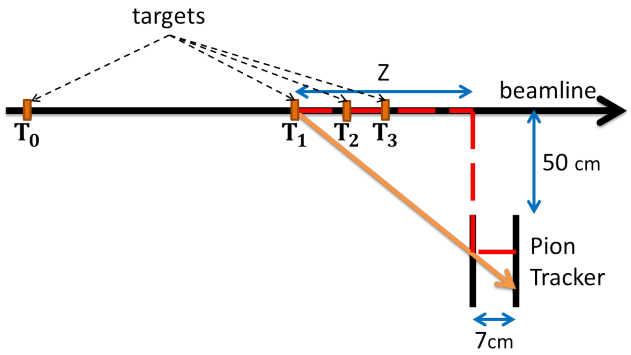

Figure 4.3: Extrapolation of angles of incident particles. With the distance to the beam line and the angles of the particles, the target positions can be reconstructed.

According to fig. 4.3 the angles of the particles and the source positions can be calculated via:

$$\begin{aligned} \tan\alpha &= \frac{\Delta x}{7\ \text{cm}} \\ Z &\approx \frac{50\ \text{cm}}{\tan\alpha} \\ \Rightarrow Z &\approx \frac{350\ \text{cm}^2}{\Delta x} \end{aligned} \tag{4.2}$$

Based on a distance of around 10 m to the FOPI target, the distances of the other sources can be determined to be 1 - 2 meters in front of the Pion Tracker. This is in perfect agreement to the real distances they had and therefore a confirmation of the statement that the other experiments act like targets. The calculated values for the angles and the distances are shown in table 4.1.

run D		
Source	angle w.r.t. beam axis	Z in m
T_0^D	1.24°	10
T_1^D	16.34°	1.9
T_2^D	21.08°	1.4
T_3^D	27.28°	1.0

run K		
Source	angle w.r.t. beam line	Z in m
T_0^K	1.55°	10
T_1^K	20.81°	1.4
T_2^K	28.01°	1.0

Table 4.1: Calculated values for the sources in the beam line. The target and the two nearest sources always had the same positions, whereas the source at 1.85 m disappeared from run D to run K.

4.2 Source Identification

According to the peaks in the position correlation (fig. 4.2), the hit correlation can be plotted with cuts on Δx and Δy. This is shown in fig. 4.4 for run K. A shift of the scintillator shadow can be seen between the two detectors which corresponds to the cuts on Δx and Δy. This implies that the blurred shape in the hit correlation (figs. 3.8 and 3.9) arised from the overlapping of several shadows. If the hit correlation is cut on the different targets, the edges, especially for Det2, are much sharper than before.
For run D it looks nearly the same (fig. 6.3 in appendix). The only difference is that the orientation of the scintillator was horizontal, so that some parts of the shape were cut away by the edges of the second detector. This is also the reason for the shrinking of the length in the histograms for the first detector, because only events with hits on both detectors are plotted.

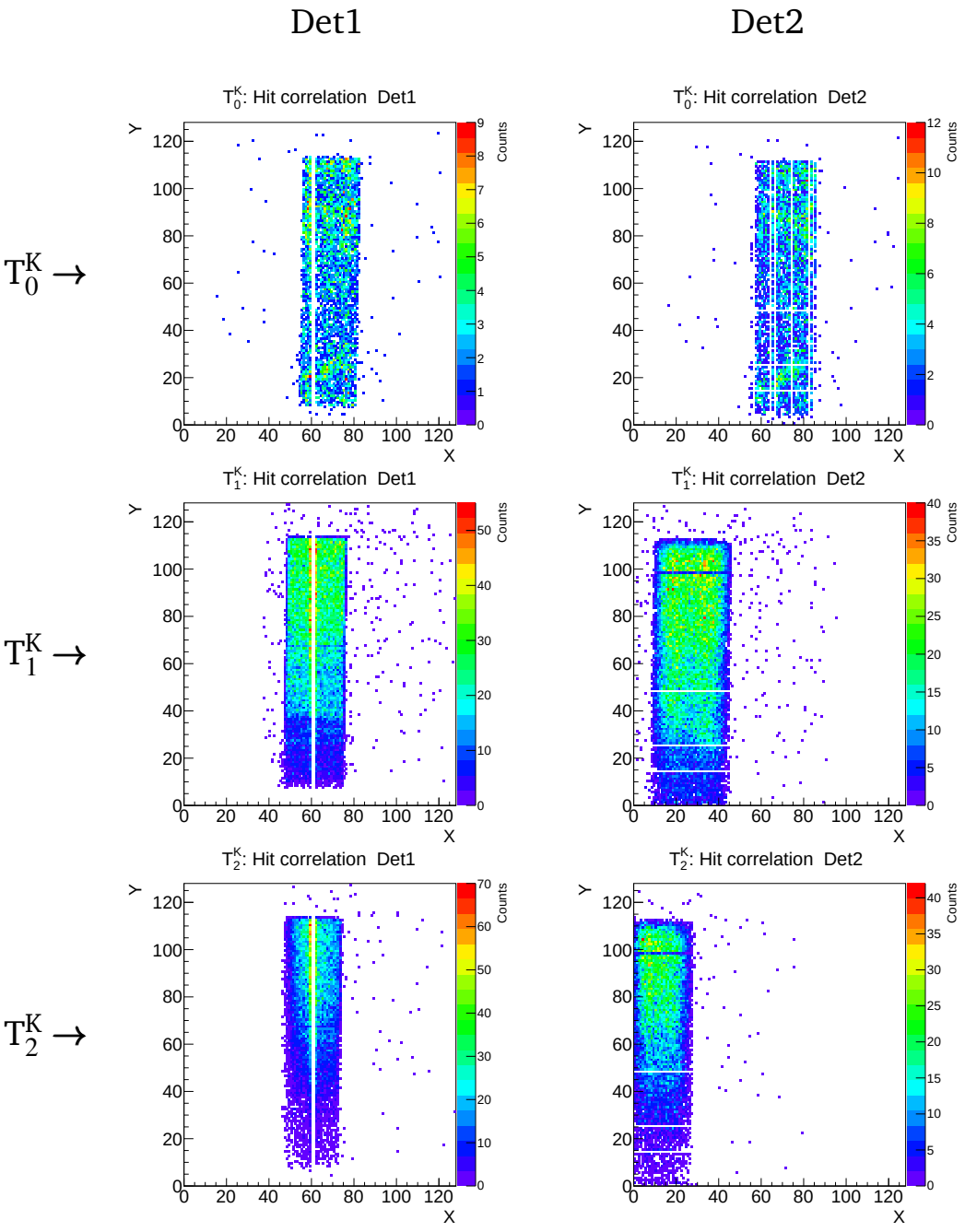

Figure 4.4: The identified sources for run K cut on Δx and Δy. The left column shows the shapes of the scintillator on the first detector and the right column the ones on the second detector. The plots are ordered from the top to the bottom according to the targets. All events here have cluster size 1.

4.3 Detector Efficiency

The detector efficiency is calculated only for the first detector. This comes from the fact that it has to be guaranteed that the particle really went through the silicon detector. Because of the setup geometry and since the particles came from different angles, it is possible that they cross the two scintillators and the first detector, but not the second one. An example for this can be seen in fig. 3.8, where the shape of the front scintillator is shifted out of the detector range for the second detector. Figure 4.5 shows a sketch for this.

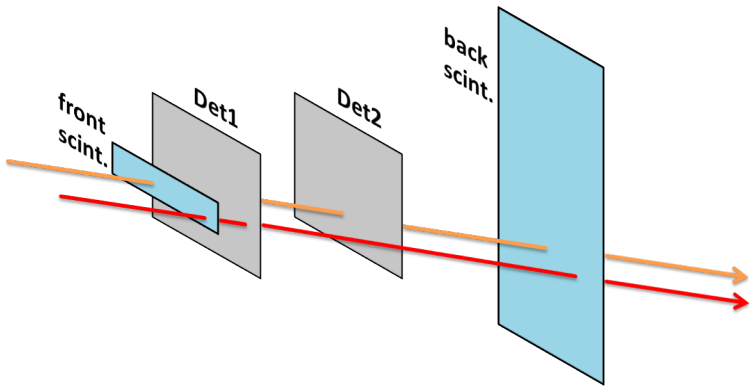

Figure 4.5: Sketch for visualizing the efficiency calculations. Two particles (red and green) are triggered by the two scintillators. Because of the setup geometry, all particles, which are triggered, have to cross the first detector. Not all triggered particles have to cross the second detector. This is due to the fact that the particles came from different angles and the bigger size of the back scintillator in comparison to the detector. Because of that the detector efficiency can only be calculated for the first detector.

All particles, which went through the front scintillator and the second detector, had to go through the first detector. So the efficiency is calculated via the number of events with at least one hit on both detectors over the number of hits in the second detector (eq. (4.3)). The & denotes a logical 'and'.

$$\text{Efficiency}^{\text{Det1}} = \frac{N^{\text{Det1}}_{\text{HM}>0} \quad \& \quad N^{\text{Det2}}_{\text{HM}>0}}{N^{\text{Det2}}_{\text{HM}>0}} \tag{4.3}$$

It shows that the efficiency for the first detector for run D is 92.0% and for run K 95.9%. But it has to be considered that there were some broken strips on the detector, where no hit could be detected. If this is taken into account, the efficiency increases. This is also the reason for the different efficiencies of 92.0% and 95.9%, because the front scintillator had in run D a horizontal and in run K a vertical orientation, and thus a different overlap with the broken strips.

Another interesting figure of merit is the track detection efficiency. This quantity shows in how much events a track could be reconstructed. So this is the number of reconstructable tracks divided by the number of events with at least one hit on both detectors (eq. (4.4)). A track can be reconstructed, if the hit multiplicity is exactly 1 for all four n-XYTER and therefore exactly one hit on each detector.

$$\text{Track detection efficiency} = \frac{N_{\text{tracks}}}{N^{\text{Det1}}_{\text{HM}>0} \quad \& \quad N^{\text{Det2}}_{\text{HM}>0}} \tag{4.4}$$

For run D it is 86.4% and 71.4% for run K. It is a smaller value for run K is because of a higher beam intensity during this run. That lead to a higher probability for more than one particle hitting the detector at the same time. These two values can be improved by a better analysis of events with multiple hits. Though this was not within the framework of this thesis. An implementation of a better track reconstruction will be done in further steps. The efficiencies are summarized in table 4.2.

	run D	run K
efficiency of the first detector	92.0%	95.9%
track detection efficiency	86.4%	71.4%

Table 4.2: Recap of all efficiencies.

4.4 Energy Spectra

The energy spectrum for both runs show a clear peak at around 150 ADC channels (fig. 4.6). This corresponds to the MIP peak in a 300 μm thick silicon layer with approximately 80 keV energy deposit. The red histogram in the plot corresponds to cluster size 1, the green one is cluster size 2 multiplied by a factor of 10 and the blue one is cluster size 3 multiplied by 10 or 100. For run D the spectra show only one huge peak in the low energy region, whereas for run K there is a second peak in the spectrum, partially overlapping with the MIP peak.

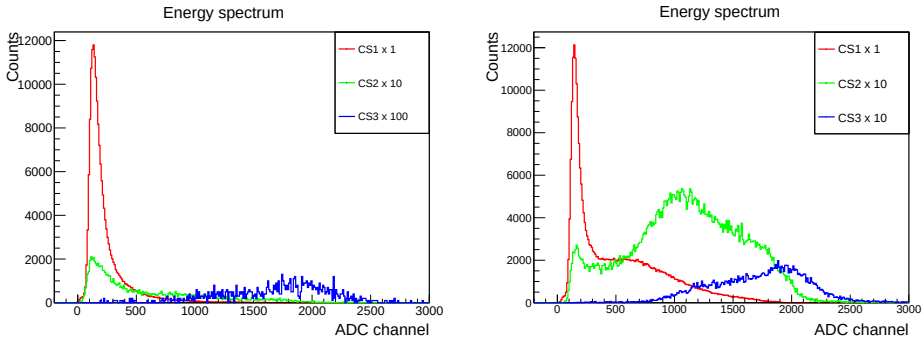

Figure 4.6: Raw energy spectra for run D (left) and run K (right). The energy spectra are plotted for different cluster sizes, which are multiplied by a weighting factor. The red peak corresponds to a MIP peak. The second peak in run K is caused by heavier fragments. The multiplication is only for visualisation.

The energy spectra can be further analysed in terms of the particles' impact angle. For this the same cuts for Δx and Δy are applied like in section 4.2. The same spectrum for run D has been plotted for different particle sources/impact angles on fig. 4.7 (for run K see fig. 4.8). It expectedly shows that the MIP peak shifts to higher ADC values and the relative ratio of cluster size 2 and 3 events increases in this region. It shows

also that nearly all the particles with high energy deposition came from the additional targets. The small shift of the peak arises from the longer track of the particle in the silicon. The length increases with 1 over the cosine of the impact angle (eq. (4.5)), and so does the deposited energy also. This behaviour for both runs is summarized in fig. 4.9.

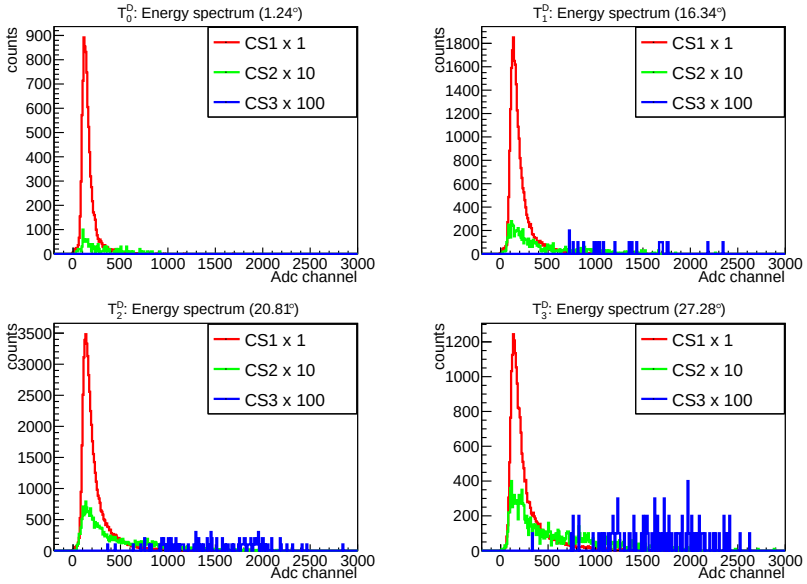

Figure 4.7: The four histograms are energy spectra cut for the different angles of incoming particles with respect to the detector plane for run D. The spectra are separated between the different cluster sizes and multiplied by a weighting factor. The multiplication is only for visualisation.

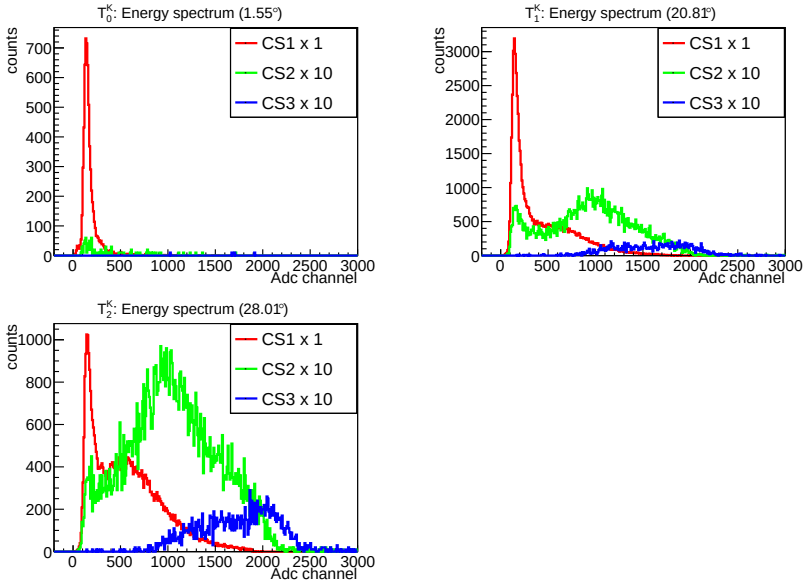

Figure 4.8: The energy spectrum cut for the different angles of incoming particles with respect to the detector plane for run K. The spectra are plotted for the different cluster sizes and multiplied by a weighting factor. The multiplication is only for visualisation.

It can be seen that for run K (green) all data points are above the ones of run D (red). Also the fit in run K, direct proportional to $1/\cos(\varphi)$, is not very good. This is due to the overlapping of the two peaks, that shifts the maximum value. In run D only the last three data points were fitted, because they can be fitted nearly perfectly. The first value is beneath the curve, but still within the errors. The fit values can be seen in table 4.3.

$$\mathrm{F}(E) = \frac{E_0}{\cos(\varphi)} \tag{4.5}$$

For further analysis only run D will be taken, because there is a clear MIP signal, which is wanted to be described. Not like in run K. There the second peak distorts the MIP signal and has a strange behaviour for bigger cluster sizes, which will not be explained in greater detail here. This behaviour is not completely understood until now.

	E_0 in ADC units	Error in ADC units
run D	130.90	0.27
run K	139.49	2.85

Table 4.3: Fitted values for the data points in fig. 4.9. The fit function is shown in eq. (4.5).

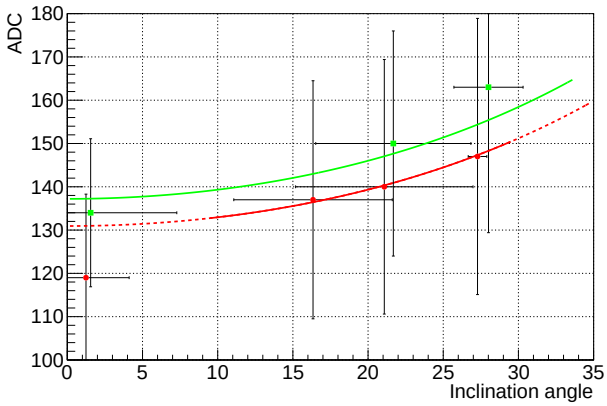

Figure 4.9: Shift of the MIP peak to higher energy values for larger angles. The data points give the mean value of the MIP peak for the particles with different impact angles. Red is run D and green is run K. The lines are fitted curves. The fit for run D is only for the last three data points. Data points are from table 4.4.

4.4.1 Cluster Size 1 Events

The MIP peak gets a little shifted to higher ADC values for larger angles and broadens a little. The values for this can be extracted from table 4.4. The mean and the sigma arise from a fit with a Landau function. The MIP peaks of the additional targets in run D are shifted to higher ADC values according to $1/\cos(\varphi)$. The difference of 18 ADC units to the FOPI target is due to the broadening. In run K the shift arises basically from the overlapping with the second peak which is caused by more ionizing particles.

run D		
Source	mean in ADC units	sigma in ADC units
T_0^D	119	19.3
T_1^D	137	27.5
T_2^D	140	29.4
T_3^D	147	31.9

run K		
peak	mean in ADC units	sigma in ADC units
T_0^K	134	17.1
T_1^K	150	26.0
T_2^K	163	33.6

Table 4.4: The fit parameters for a Landau fit of the MIP peak of cluster size 1 events for figs. 4.7 and 4.8. The values are listed for the different particle sources.

4.4.2 Cluster Size 2 Events

The MIP peak gets a relative increase at larger angles in comparison to cluster size 1 events and the maximum shifts also to higher energies. In run K the second peak in T_1^K and T_2^K also appears, but at higher values than the one for cluster size 1. It is also a very broad peak. To get a better understanding of the two peaks, two plots were made (fig. 4.10). They show both the sharing of the energy in the two strips. In the left histogram the ADC value in one strip is plotted against the ADC value in the other strip. So the total energy increases from the bottom left corner to the top right corner. One can see a peak in the small energy region corresponding to the MIPS and two rather long peaks parallel to the axis. This shows that for higher energy regions the created charge is split up unevenly. In the right histogram one can see the total energy as a function of the proportionally deposited energy in one strip. 0 and 1 are adequate with a cluster size 1 event, where one strip takes the whole created charge. The more nearer the value is to 0.5, the more equal the charge is shared. It shows that in the MIP region it is rather likely to split the energy uniformly, whereas at high energies the most of the charge is deposited in one strip.

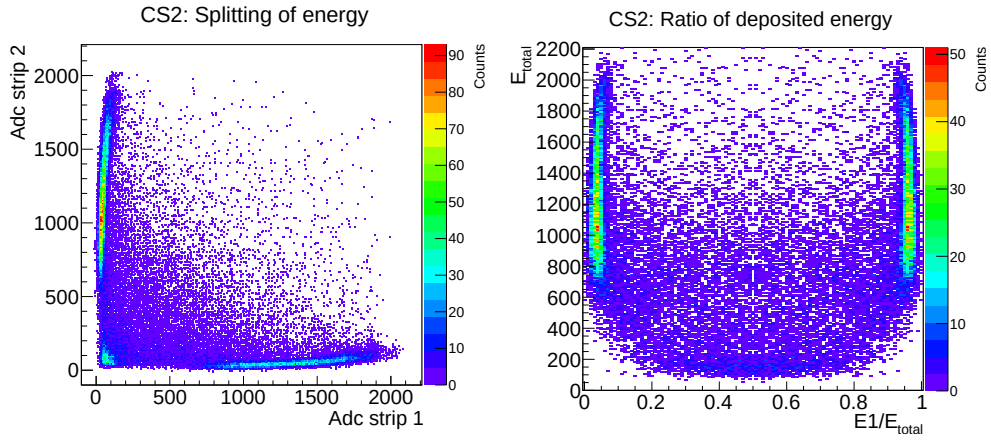

Figure 4.10: Charge sharing in CS2 events for run K. Both show a unequal sharing of the charge at high energies. Left: Total energy as a function of the proportionally deposited energy in one strip.
Right: In one strip deposited energy versus in second strip deposited energy. The MIP peak is in the bottom left corner.

In the small energy region between 0 and around 400 ADC units in total energy, the MIPs do a quite equally sharing of the charge. Whereas in the high energy region between 600 and 2200 ADC units, in most of the cases 93% of the charge is collected on one strip. Since the particles with high energy loss have mostly bigger angles, such a behaviour is rather unlikely. This effect is not well understood, so that more investigations have to be done.

4.4.3 Cluster Size 3 Events

Like in cluster size 1 and 2 events, here is also a broad second peak in the two large angles of run K. The mean of this is shifted again to still higher ADC values. For run D are also some events for the nearer sources.
In this case the charge sharing by a particle crossing three strips is suppressed, since they would have to have an angle of approximately 79° (eq. (4.6)).

$$\tan(\alpha) \approx \frac{2 * 760\mu\text{m}}{300\mu\text{m}} \qquad \alpha \approx 79^\circ \tag{4.6}$$

For such huge angles, the particle would not cross both trigger scintillators. So it had to be two or more particles crossing the detector nearby, or it is also caused by the effect described above, which is not totally understood.
To separate these two types, one has to look at the pattern of cluster size 3 events. Here one labels the strips with the numbers 1,2,3 according to the deposited energy in the strip (fig. 4.11 left). The order of the number creates a pattern. The frequency of each pattern is plotted on the right hand side of fig. 4.11.

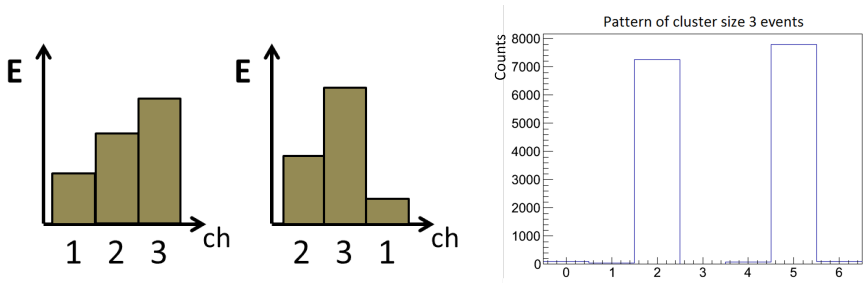

Figure 4.11: Pattern for cluster size 3 events. On the left hand side a scheme how the pattern comes about. On the right hand side the frequency of all patterns for run K in the x-direction on the second detector.

The events with 1 or 2 in the middle have to be two nearby particles. The other ones are not well understood. It would also be possible that more than two particles crossed the detector nearby, but for this the already low probability would decrease by orders of magnitude. Therefore such events can be neglected.

Figure 4.12 shows the deposited energy in the three neighbouring strips. The two outermost strips have basically a signal at small energies, whereas the middle strip has a small peak at low and a big peak high energies. The big peak at high ADC channels corresponds to events with pattern '132' and '231' and the small left peak to the other ones. The sharp edge at around 2000 ADC channels in the middle histogram is caused by a saturation level of the silicon detector.

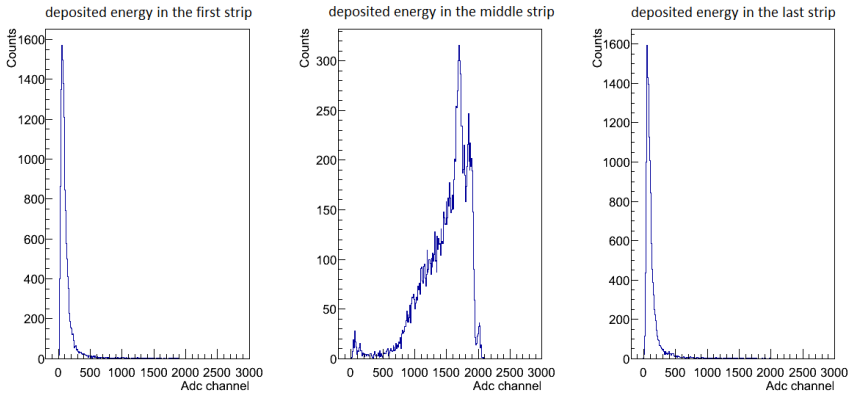

Figure 4.12: Partitioning of energy to the three strips in cluster size 3 events. The histograms are ordered exactly like the fired strips.

4.5 Probability for Charge Sharing

The relevant part for the pion beam is the MIP region. So a distribution has to be found, which describes the probability of charge sharing under different angles.
From geometrical considerations the angle of particles cannot be larger than 55° because of the size and the distance of both of the silicon detectors. This is much smaller than a track going through three strips so that only cluster sizes 1 and 2 have to be considered.

The probability for charge sharing can be calculated also with geometrical considerations. The active strip area of the detector is $97,22 \times 97,22$ mm^2 with 128 strips. Since it is a continuous silicon layer, a strip is defined by the electric field, created by the doping (fig. 4.13).

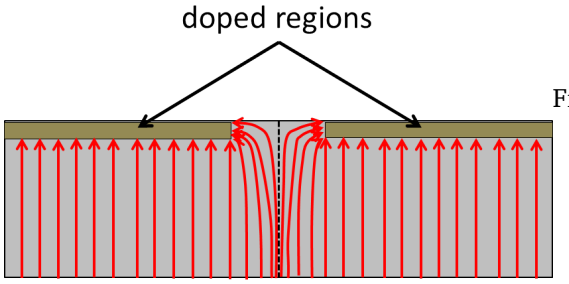

Figure 4.13: Electric field in a striped silicon detector. The red lines are the electric field lies.

The electron-hole pairs, created by energy deposition, move in opposite directions according to the electric field. Therefore one n-XYTER gets the signals from the electrons, the other one from the holes, produced on the whole track of a particle through the silicon. For the following calculations only one detector side, so only electrons or holes, are taken into account. The whole concept can be applied independently on both sides of the strip detector.
In an effective model for describing the charge sharing effect, one can assume a small volume between two strips, where the created charge is nearly equally split up between the two. This area is defined by the parameter s (fig. 4.14). So the split-up volume is p-2s wide and because of that, the length l of each strip is increased by 2s. One reason for this is that the electron-hole pairs are not created exactly on the track line, but distributed around it in a certain range of a few micrometers [11]. The other reason is that the created charge has kinetic energy, and so can overcome the electric potential to get into the neighbouring strip.

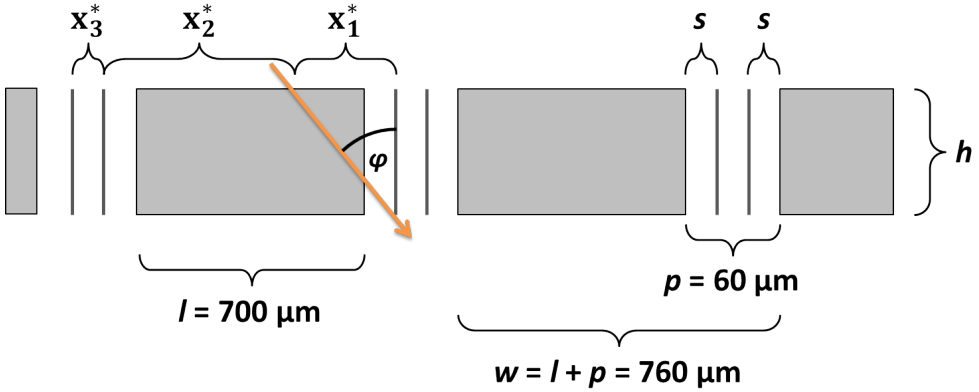

Figure 4.14: Sketch for calculating the charge sharing. From the company the strip width and the strip pitch are given. They are $l = 700$ μm and $p = 60$ μm [7]. In practice the silicon is a continuous layer, so that it can be described by an effective model. The particle goes straight through the detector with an angle φ. The parameter s defines the split-up volume and x_1^*, x_2^*, x_3^* are some ranges relevant for the calculation. The * means that no minimum track distance is required, to produce a signal above the threshold.

For calculating the charge sharing the strip width w is split up into 3 regions, x_1^*, x_2^* and x_3^*. Assuming a particle, under a certain angle φ, needs only an infinitesimal short track in the silicon to get detected. Then the regions x_1^* and x_3^* would correspond to the charge sharing and thus cluster size 2. If it hits the detector in region x_2^*, then only one strip fires.
This model is only defined up to angles $\varphi \approx 66°$ because then the cluster size 3 would have to be considered. But this is not relevant at all since such huge angles would not be triggered anyway and maximum 55°can be reached due to the sizes of the detectors.

It follows that the probability for cluster size 2 is:

$$P = \frac{x_1^* + x_3^*}{x_1^* + x_2^* + x_3^*} \tag{4.7}$$

$$\frac{x_1^*}{h} = \tan\varphi \qquad \Rightarrow \qquad x_1^* = h \cdot \tan\varphi \tag{4.8}$$

$$x_3^* = p - 2 \cdots \tag{4.9}$$

$$\Rightarrow P = \frac{h \cdot \tan\varphi + p - 2 \cdot s}{l + p} \tag{4.10}$$

$$\boxed{P = \frac{h}{w} \cdot \tan\varphi + \frac{p - 2 \cdot s}{w}} \tag{4.11}$$

This shows that the probability increases with φ, proportional to the tangent. There is also a small offset proportional to s. This offset is the minimum probability for cluster size 2, which can be determined at $\varphi = 0°$.

Up to now no minimum track distance is required for producing enough charge to make a signal above the threshold. This can be changed by implementing a minimum track distance c, which is indirectly proportional to the energy loss of the particle.

$$c = E_{\text{cut}} \cdot \left(\frac{\mathrm{d}E}{\mathrm{d}x}\right)^{-1} \tag{4.12}$$

Where E_{cut} is equivalent to the set threshold.

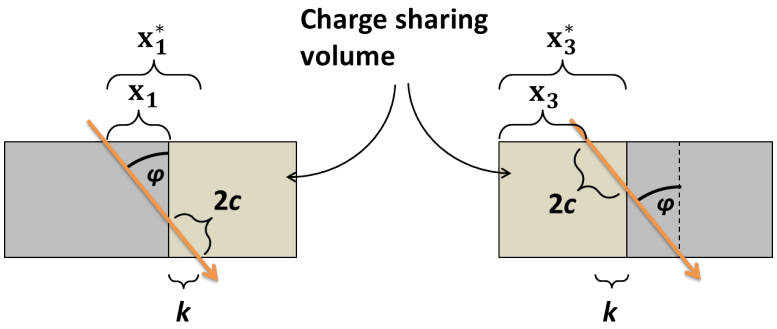

Figure 4.15: Sketch for the minimum track length in silicon. The regions x_1^* and x_3^* shrink according to the minimum track length c. Here it is $2c$, because it's in the split-up volume. The values x_1 and x_3 are after applying the E_{cut}.

Figure 4.15 shows a sketch of how c can be implemented. A signal is registered if the deposited energy is higher than E_{cut}. For cluster size 2 the minimum track distance has only to be considered in the split-up volume, because if the deposited energy is enough, both strips will fire anyway, no matter how long the track in the strip is. This means a track length of $2c$ for the split-up volume, because the two neighbouring strips get only half of the signal. From a c>0 follows a shift of the track in the sketch and so a

reducing of the values x_1^* and x_3^* to x_1 and x_3. This leads to a decrease in the probability for cluster size 2 depending on the angel φ. The length k represents the shift of the track and reduces x_1^* and x_3^*.

$$\frac{k}{2c} = \sin\varphi \tag{4.13}$$

$$\Rightarrow \quad \begin{aligned} x_1 &= x_1^* - k = x_1^* - 2c \cdot \sin\varphi \\ x_3 &= x_3^* - k = x_3^* - 2c \cdot \sin\varphi \end{aligned} \tag{4.14}$$

With a constant width w the final formula for the probability is:

$$\boxed{P = \frac{h}{w} \cdot \tan\varphi + \frac{p - 2 \cdot s}{w} - \frac{4c}{w} \cdot \sin\varphi} \tag{4.15}$$

Here there is obviously no inclination angle along the strips included. This would lead to an additional factor of $\cos\theta$ in the the $\sin\varphi$ term. For the x-direction (Nx0 and Nx2) θ is maximum 5.3° so $\cos\theta \approx 0.996$. This can be neglected. For the y-direction (Nx1 and Nx3) the θ angle would be between 0°and 28°, so that this cannot be neglected. Because of this the y-direction will not be considered in the fits because the additional parameter and error would make a non precise fit (fits from figs. 4.16 and 4.17).

The measuring points for this formula can be extracted from the energy spectra in figs. 4.7 and 4.8. The angles are determined by the position correlation plot like in table 4.1 and the probability at the different angles comes from the ratio of events with cluster size 2 over the total amount of events in the energy spectra. For this only the small energy range around the MIP peak up to 300 ADC channels was considered, because otherwise the measurement gets distorted for run K by events within the second peak. All the measuring points are listed in table 4.5.

The extracted data can be put in a graph and eq. (4.15) can be fitted through these points. The result is plotted in figs. 4.16 and 4.17. It shows that this formula describes the data very well.
The magenta curve is the same for both runs. It is a theoretical curve with fixed parameters. The height h was set to 300 μm, the real size of the silicon. The parameter s was estimated to 25 μm, which equates to a 10 μm thick split-up volume and the minimum track length was set to 45 μm. Besides the height, all parameters were only estimated, but seem to be in an adequate region. This provides a feeling of the probability's behaviour and a flavour for the order of magnitude the probabilities should have.
The black (Nx0) and green (Nx2) curves for each run are the fits to the corresponding data points. Here the height h was set to 300 μm, but it can be also set to be variable, so that it gets also fitted. This would be necessary for either an unknown size of the silicon, or a not perfectly working silicon detector, where a depletion zone exists and hence not all created charge gets registered. The values for the several parameters are listed in table 4.6.

run D

Source	inclination angle	probability Nx0	probability Nx2
T_0^D	1.24°	0.95%	2.12%
T_1^D	16.34°	1.88%	2.78%
T_2^D	21.08°	2.74%	3.36%
T_3^D	27.28°	3.54%	4.42%

run K

Source	inclination angle	probability Nx0	probability Nx2
T_0^K	1.55°	0.80%	1.88%
T_1^K	20.81°	2.91%	2.98%
T_2^k	28.01°	4.39%	4.09%

Table 4.5: Measuring points for the angular distribution of cluster size 2 events. The angles are calculated via the Δx from the position correlation plot. The probabilities are the number of cluster size 2 events, over the total number of events in the MIP region for the different angles (figs. 4.7 and 4.8).

The two plots (figs. 4.16 and 4.17) show that the real behaviour is quite close to the theoretical one. There is a non vanishing probability for charge sharing at 0° of around 1-2% and a increase for larger angles. The relatively good description of the data by eq. (4.15) shows that an effective model for charge sharing is a good approach. As seen in table 4.6, the two detectors have slightly different properties, which are consistent within the errors for both runs. The minimum track length is nearly the same for both detectors and the split-up volume is about 20% larger for the second than for the first detector.

	run D		run K	
	Nx0	Nx2	Nx0	Nx2
h (in μm)	300	300	300	300
s (in μm)	26.5 ± 0.6	22.0 ± 0.7	27.2 ± 1.2	22.8 ± 0.8
c (in μm)	71.6 ± 3.4	73.9 ± 3.0	70.0 ± 3.1	75.8 ± 2.5

Table 4.6: Fitted parameters for both runs in x-direction (Nx0 and Nx2). Nx2 corresponds to the first detector and Nx0 to the second detector.

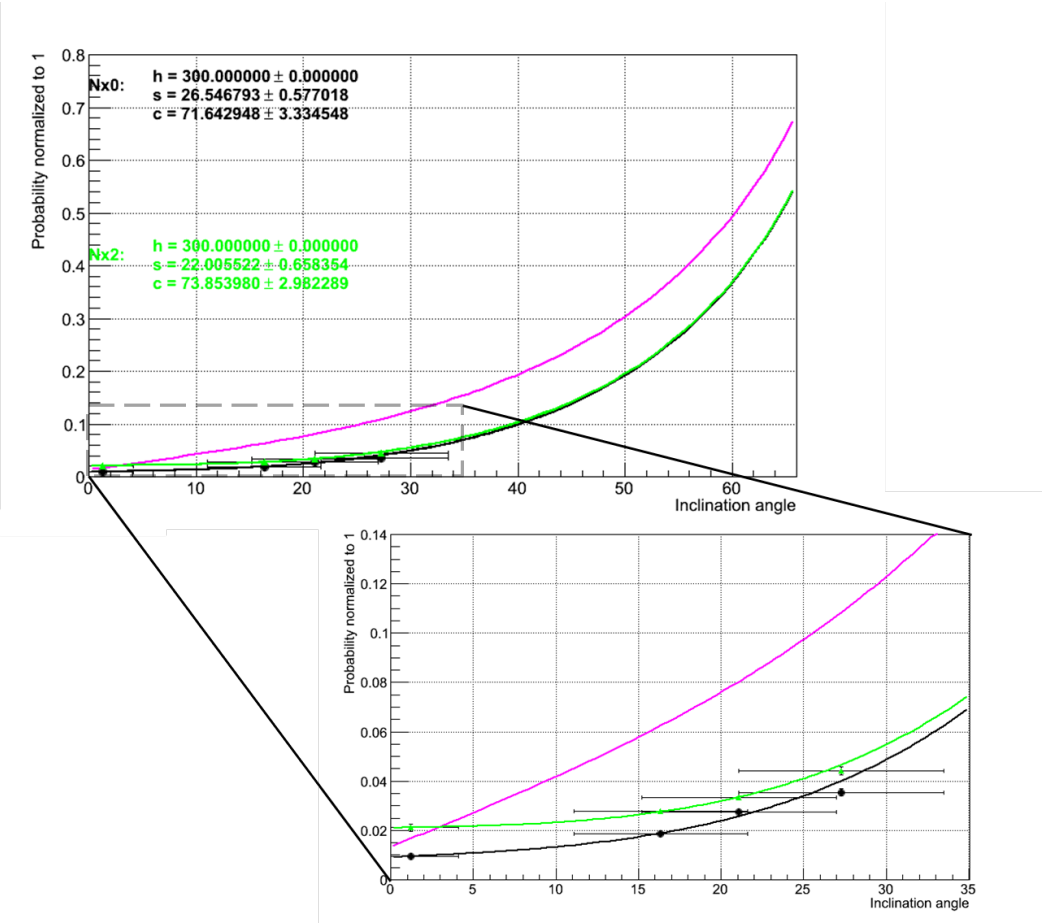

Figure 4.16: Fitted charge sharing distribution for run D. In the top is the full range from 0° to 66°. In the bottom is a zoom in the relevant region. Black and green are the fitted curves for the x-direction (Nx0 and Nx2) and magenta is a theoretical curve with estimated parameters.

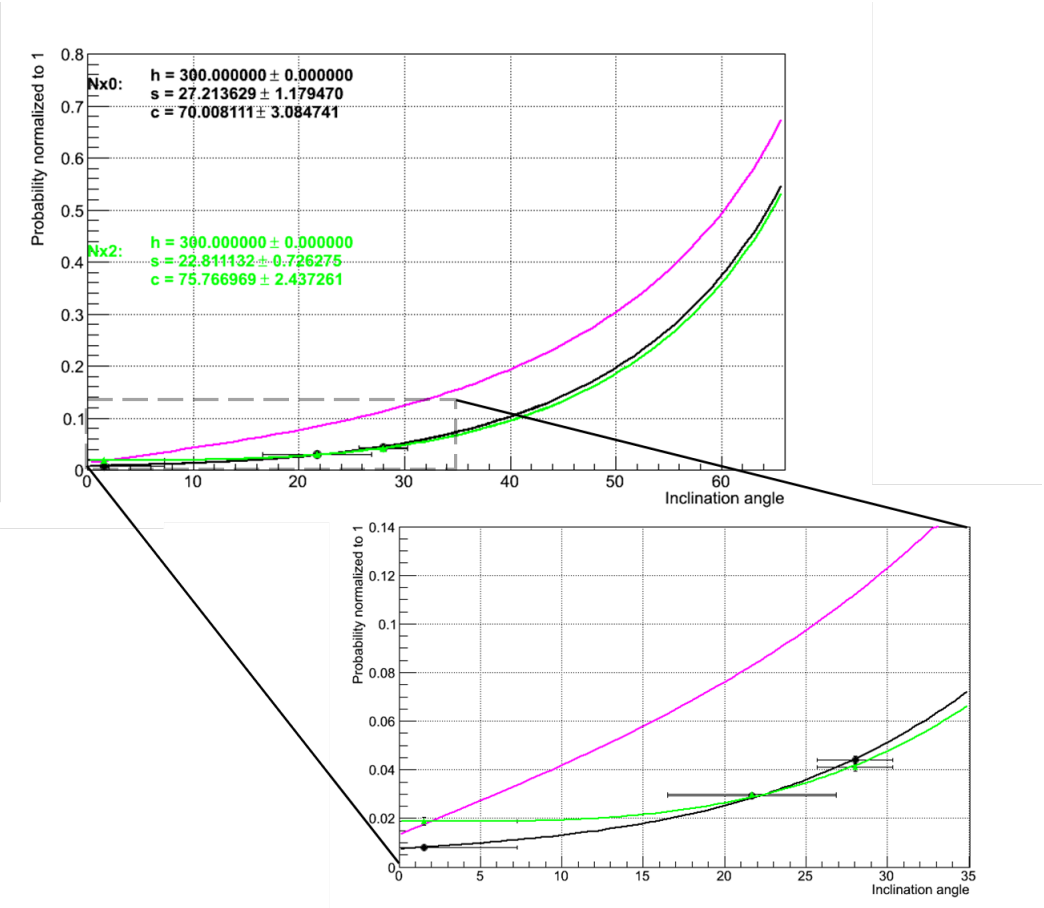

Figure 4.17: Fitted charge sharing distribution for run K. In the top is the full range from 0° to 66°. In the bottom is a zoom in the relevant region. Black and green are the fitted curves for the x-direction (Nx0 and Nx2) and magenta is a theoretical curve with estimated parameters.

5 Summary, Conclusion and Outlook

Summary

This thesis presented an overview about the actual analysis of test data for a prototype of the HADES Pion Tracker. The data had been taken in 2012 at GSI in Darmstadt with secondary particles produced in fixed target collisions. First the raw data was analysed, to show that the detector system works fine. A deeper look into the data showed the existence of several targets along the beam line, from which the particles came under different angles to the detector. After that an effective model for the charge sharing effect was deduced. Together with energy spectra, a charge sharing effect dependent on the incident angle of particles was observed. It showed that this effect lies within 1-2% for very small angles and is therefore not negligible for the later pion beam experiments. But since the detection for MIPs works even for cluster size 2 events completely unproblematic, this forms no obstacle.

Conclusion

The results from section 4.5 show that the charge sharing effect in a striped silicon detector can be described by an effective model. In the angular range,relevant for the pion beam, there is up to 1.2°, a non vanishing probability to split the created charge into two strips. The probability for that is around 1-2%. This is a non negligible part, which therefore has to be considered. But, like shown in section 4.4, the Pion Tracker is able to detect MIPs which undergo charge sharing.
All in all, one can say that the Pion Tracker is fully capable to detect MIPs and thus no conceptual changes have to be made.

Outlook

For better determination of the angular dependence of charge sharing, especially in the big angle region, more measurements under a number of angles would be required. A more detailed analysis of the existing data could also provide better results. An implementation of a "real cluster finder" code, written by Rafał Lalik, is foreseen. This algorithm provides the handling of hit multiplicities higher than 1. It can iterate over all possible tracks and decide which are the right ones. This will improve the track efficiency of the detector system, so that fewer events have to be cut away.
Also new beam tests with a more sophisticated prototype at COSY[15] in Jülich in December 2013 are planned. There the detector with perhaps cooling and with TRB3 [3] in a full readout chain will be tested. In the high beam rate tests, the detector, the n-XYTER and the DAQ efficiency are going to be examined.

[15] Cooler Synchrotron

6 Appendix

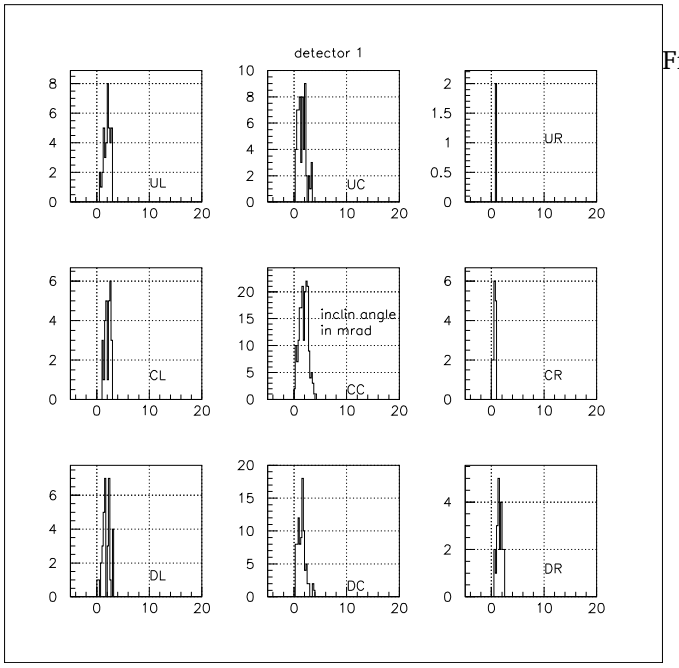

Figure 6.1: Simulated inclination angle of the pions on the first detector. Angle on the X-axis in mrad and counts on Y-axis. Angle is always smaller than 4 mrad on whole detector. UL means upper left corner, CL center left, etc.. The different pictures show different positions on the detector.
UL: Y= 0.8 cm, X= -2.5 cm; UC : Y= 0.8 cm, X= 0.0 cm; UR : Y= 0.8 cm, X= 2.5 cm; etc. Picture made by Thierry Hennino.

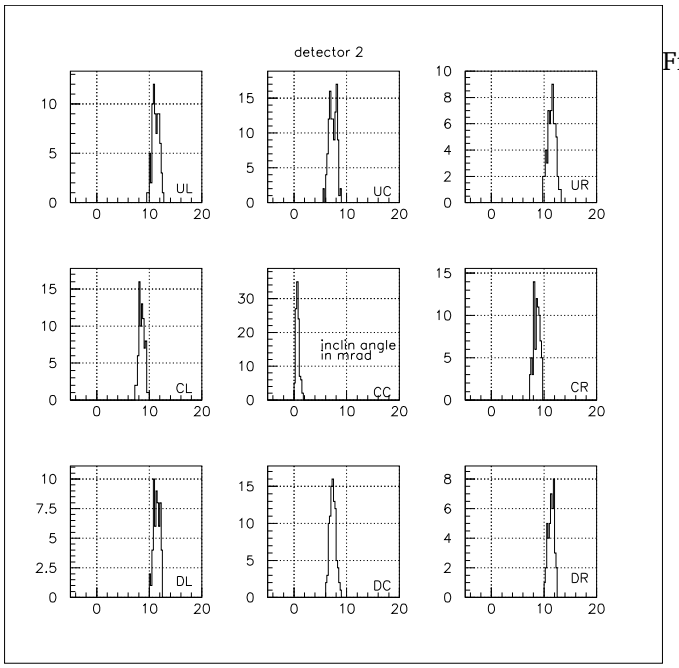

Figure 6.2: Simulated inclination angle of the pions on the second detector. Angle on the X-axis in mrad and counts on Y-axis. Angle is always smaller than 20 mrad on whole detector. UL means upper left corner, CL center left, etc. The different pictures show different positions on the detector.
UL: Y= 3.0 cm, X= -3.0 cm; UC : Y= 3.0 cm, X= 0.0 cm; UR : Y= 3.0 cm, X= 2.5 cm; etc. Picture made by Thierry Hennino.

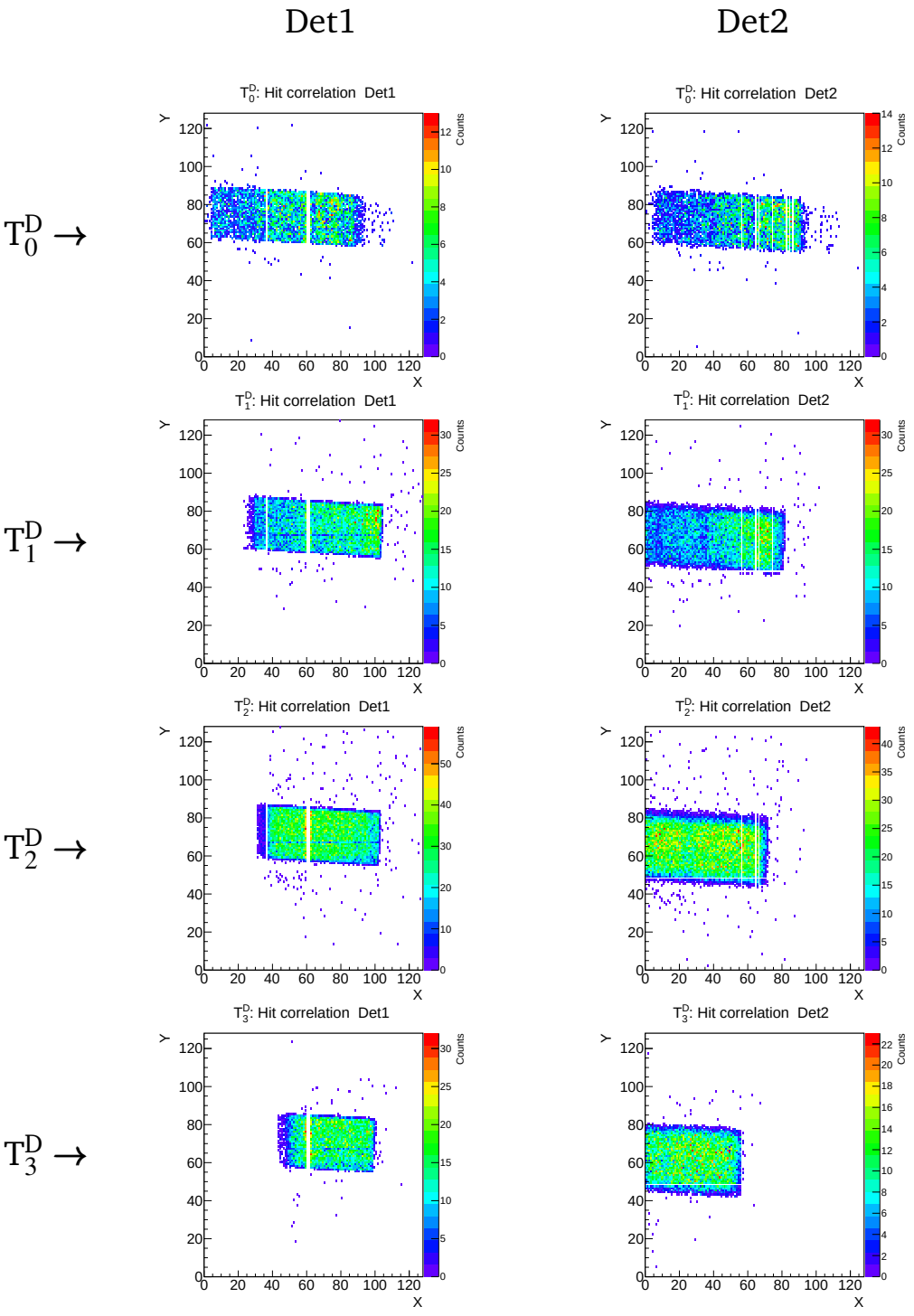

Figure 6.3: The identified sources for run D cut on Δx and Δy. The left column shows the shapes of the scintillator on first detector and the right column the ones of the second detector. The plots are ordered from the top to the bottom according to the targets. All events here have cluster size 1.

References

[1] HADES collaboration. The high acceptance dielectron spectrometer HADES. *The europeam physics journal A*, page 2, 2009. URL http://hades-new.gsi.de/sites/default/files/web/media/documents/\EPJA2009.pdf. visited on: 18.07.2013.

[2] Lapidus K. Interactions between strange and plain matter, 07 2013.

[3] Fabbietti L. et al. A secondary Pion Beam for the HADES Experiment: Technical Design Report. HADES collaboration, 07 2013. URL http://www.e12.ph.tum.de/~rlalik/HADES_Cerberos_TDR.pdf. visited on 23.07.2013.

[4] Wirth J. Development of a cooling system for a silicon particle detector. Bachelor thesis, TU München, 06 2012. URL http://www.e12.ph.tum.de/groups/kcluster/Documents/Publications/bachelorthesis_joana_wirth.pdf. visited on: 18.07.2013.

[5] Louis P. Entwicklung eines Kühlsystems für einen Silizium-Detektor. 2013.

[6] Shin Watanabe Hiroyasu Tajima Takaaki Tanaka Kazuhiro Nakazawa Shin'ichiro Takeda, Tadayuki Takahashi and Yasushi Fukazawa. Double-sided silicon strip detector for x-ray imaging, 02 2008. URL http://spie.org/x20060.xml. visited on 17.07.2013.

[7] Micron semiconductor ltd. *AC & DC COUPLED ION IMPLANTED TOTALLY DEPLETED DOUBLE SIDED 90° MICROSTRIP DETECTOR WITH GUARD RINGS*. Micron semiconductor ltd, 2011. URL http://www.micronsemiconductor.co.uk/pdf/ttt.pdf. visited on: 07.07.2013.

[8] Saint-Gobain Chrystals. *BC-400,BC-404,BC-408,BC-412,BC-416 Premium plastic scintillators*. Saint-Gobain Chrystals, 07 2008. URL http://www.detectors.saint-gobain.com/uploadedFiles/SGdetectors/\Documents/Product_Data_Sheets/BC400-404-408-412-416-Data-Sheet.pdf. visited on: 07.07.2013.

[9] Friedl L. *The CMS Silicon Strip Tracker and it's Electronic Readout*. PhD thesis, Vienna University, 2001. URL http://www.hephy.at/user/friedl/diss/diss.pdf. visited on: 17.07.2013.

[10] Lalik R. Development of the Pion Tracker for HADES spectrometer, 03 2013. URL http://www.e12.ph.tum.de/~rlalik/DPG13.pdf. visited on: 18.07.2013.

[11] Mazziotta M. N. A full Monte Carlo simulation code for silicon strip detectors, may 2004. URL http://www.docstoc.com/docs/120731848/A-full-Monte-Carlo-simulation\-code-for-silicon-strip-detectors. visited on: 18.07.2013.

List of Figures

Acknowledgement

There are a number of people to whom I am grateful for their help throughout the course of my thesis. I would like to thank especially,

First of all, Professor Dr. Laura Fabbietti for giving me the chance to work in her group and for granting me this interesting thesis topic;

Rafał Lalik, my supervisor, for his continued support and competent advice during my thesis work. I benefited from his expert knowledge, which he shared kindly;

All the members of our group, which helped me at any moment, when I had a question;

My bachelor colleagues, with which I had a lot of fun.

Meiner Freundin Franziska Müller, die mir ihre volle Unterstützung während der Zeit an dieser Abschlussarbeit gab, auch wenn ich ziemlich beschäftigt war und nicht viel Zeit für sie hatte.

Meinen Eltern, für ihre finanzielle und moralische Unterstützung während meiner bisherigen Studienzeit.